Available online at www.sciencedirect.com
ScienceDirect
Earth and Planetary Science Letters 268 (2008) 268–282
EPSL
www.elsevier.com/locate/epsl

Olivine fabric transitions and shear wave anisotropy in the Ryukyu subduction system

Erik A. Kneller [a,*], Maureen D. Long [b], Peter E. van Keken [a]

[a] Department of Geological Sciences, 1100 North University Ave., University of Michigan, Ann Arbor, MI 48109-1005, USA
[b] Department of Terrestrial Magnetism, 5241 Broad Branch Road, Carnegie, Institution of Washington, Washington, DC 20015-1305, USA

Received 19 May 2007; received in revised form 20 September 2007; accepted 5 January 2008
Available online 26 January 2008
Editor: G.D. Price

Abstract

Recent shear wave splitting measurements from the fore-arc region of the Ryukyu subduction system show large magnitude (0.3–1.6 s) trench-parallel splitting in both local and teleseismic phases. The similarity of splitting parameters associated with shallow local-S and teleseismic phases suggests that the source of anisotropy is located in the fore-arc mantle. One explanation for this pattern of shear wave splitting involves a transition from commonly observed high-temperature olivine fabrics with flow-parallel seismically fast directions to a flow-normal B-type olivine fabric in the cold fore-arc mantle of the Ryukyu wedge. We test the B-type fabric hypothesis by comparing observed splitting parameters to those predicted from geodynamic models that incorporate olivine fabric development. The distribution of olivine fabric is calculated with high-resolution thermomechanical models of the Ryukyu subduction zone that include realistic slab geometry and an experimentally based wet olivine rheology. We conclude that B-type fabric can explain the magnitude and trench-parallel orientation of deep local-S phases that sample the core of the fore-arc mantle. However, our calculations show that B-type fabric alone cannot account for large magnitude trench-parallel splitting associated with teleseismic phases that sample the shallow tip of the fore-arc mantle. Alternative models for trench-parallel teleseismic splitting in the shallow tip of the fore-arc mantle involve the addition of crustal or slab anisotropy and highly anisotropic foliated antigorite serpentinite.

Keywords: shear wave splitting; subduction zone modeling; olivine fabric; non-Newtonian rheology

1. Introduction

Recently, Long and van der Hilst (2005, 2006) investigated seismic anisotropy beneath fore-arc islands of the Ryukyu subduction system using stations from F-net, a broadband seismic network administered by the Japanese National Research Institute for Earth Science and Disaster Prevention (NIED) (http://www.fnet.bosai.go.jp). They measured shear wave splitting associated with both teleseismic and local-S phases and observed trench-parallel fast directions along the entire arc with maximum delay times of greater than 1 s. Ray paths of both teleseismic and local-S phases intersect the cold corner of the mantle wedge with a range of backazimuths and reveal the 3-D structure of seismic anisotropy.

This splitting pattern is similar to the trench-parallel pattern that is seen in many subduction zones (Yang et al., 1995; Smith et al., 2001; Nakajima and Hasegawa, 2004; Long and van der Hilst, 2005, 2006; Anderson et al., 2004; Nakajima et al., 2006). Such observations are unexpected since models of 2-D wedge flow in subduction zones with A-type olivine fabric are associated with fast seismic anisotropy perpendicular to the trench (or parallel to plate motion) (McKenzie, 1979). This has led to the development of several models of mantle wedge anisotropy that include 3-D flow (Buttles and Olson, 1998; Hall et al., 2000; Kneller and van Keken, in revision), melt-related anisotropy (Hiramatsu et al., 1998; Fischer et al., 2000; Holtzman et al., 2003), and olivine fabric transitions (Kneller et al., 2005, 2007; Lassak et al., 2006; Long et al., 2007).

* Corresponding author. Tel.: +1 734 763 4069; fax: +1 734 763 4690.
E-mail address: ekneller@umich.edu (E.A. Kneller).

0012-821X/$ - see front matter © 2008 Elsevier B.V. All rights reserved.
doi:10.1016/j.epsl.2008.01.004

Recent deformation experiments show that olivine lattice preferred orientation (LPO) is a function of water content, stress, and temperature. Most olivine LPO observed in nature and in the laboratory is associated with a seismically fast direction that aligns parallel to the flow direction (Ismaïl and Mainprice, 1998). However, experiments show that at relatively high-stress and wet conditions the seismically fast direction aligns perpendicular to the flow direction, giving rise to B-type olivine fabric (Jung and Karato, 2001; Jung et al., 2006; Katayama et al., 2005; Katayama and Karato, 2006). Katayama and Karato (2006) developed a theoretical fabric-transition model for B- and C-type fabrics. This model is constrained by both experimental and natural observations (Katayama et al., 2005; Frese et al., 2003; Mizukami et al., 2004; Skemer et al., 2006) and shows that transition shear stress increases linearly with temperature. A linear extrapolation of the fabric transition from high-stress experimental conditions to the low-stress conditions more suitable for the mantle suggests that the transition temperature for B-type fabric is around 650–900 °C. This range of temperature is consistent with inferred temperatures for natural B-type fabric (Skemer et al., 2006).

Geodynamic subduction zone models with experimentally based wet olivine rheology and fabric transitions show that B-type fabric conditions are localized in the fore-arc mantle of subduction zones (Kneller et al., 2005, 2007). This predicted distribution of flow-perpendicular olivine fabric coincides with the inferred location of the anisotropic source responsible for trench-parallel shear wave splitting in the Ryukyu subduction system. This B-type fabric hypothesis is considered the mostly likely cause of trench-parallel anisotropy in the Ryukyu subduction system by Long and van der Hilst (2006) and does not require complex 3-D deformation in the cold corner of the mantle wedge. In this work we test the applicability of the B-type olivine fabric hypothesis to observations from the Ryukyu system with geodynamic models of subduction and olivine fabric development.

2. Geologic and tectonic setting

The Ryukyu subduction system is associated with westward subduction of the oceanic Philippine Sea Plate beneath the continental Amurian plate and South China block (Kubo and Fukuyama, 2003; Nishimura et al., 2004; Taira, 2001) (Fig. 1a). The main tectonic units of this system include (1) the Okinawa trough, which is a continental back-arc rift zone, (2) an elevated arc composed of parallel island chains built on a basement of pre-Miocene accretionary materials, (3) an accretionary wedge that thins toward the south, and (4) a trench with a maximum depth of 6.5 km (Iwasaki et al., 1990). The inner row of islands consists of Quaternary volcanic centers and tapers off in the central and southern parts of the subduction system (Shinjo, 1999; Shinjo et al., 2000). The outer island chain consists of non-volcanic fore-arc outcrops made up of mostly accretionary materials with minor limestone and granite (Faure et al., 1988; Ujiie, 2002). The thickness of the continental crust in the overriding plate increases toward the south and ranges from 25 to 30 km (Iwasaki et al., 1990; Kodaira et al., 1996).

The Ryukyu arc is divided into northern, central, and southern sections, with boundaries defined by left-lateral strike slip faults (Tokara Channel in the north and Kerama Gap in the south) oriented perpendicular to the trench (Kodaira et al., 1996) (Fig. 1a). In the northern and central regions relative convergence between the Philippine Sea plate and fore arc is orthogonal (Nishimura et al., 2004). In the southern region trench curvature increases and convergence becomes increasingly oblique. An active volcanic arc is located in the northern part of the Ryukyu system. However, only three Quaternary volcanic centers are located in the central and southern regions.

Fault geometry and focal mechanisms from shallow earthquakes throughout the Ryukyu system suggest that the stress field is dominated by oblique to trench-perpendicular extensional stress in the Okinawa trough and trench-parallel extension in the fore arc (Kubo and Fukuyama, 2003; Fournier and Fabbri, 2001). GPS observations show that the fore arc of the Ryukyu system is moving south relative to Eurasia and that trench-parallel extension occurs in the fore arc (Nishimura et al., 2004; Nakamura, 2004). These observations are consistent with back-arc rifting in the Okinawa trough, which started 7 Ma (Kamata and Kodama, 1999), and slow slab rollback. Although the fore arc is undergoing trench-parallel extension associated with slab rollback (Kubo and Fukuyama, 2003), the magnitude of trench-parallel stretching that has accumulated since the incipient stages of back-arc rifting is less than 20%. This magnitude of strain is not sufficient to significantly modify strain geometry in the fore-arc and arc mantle.

In the northern part of the system the Wadati–Benioff zone is relatively steep and the state of stress in the down going slab is predominately down-dip extension (Kubo and Fukuyama, 2003). Here the age of the down-going oceanic lithosphere ranges from 25 to 35 Myr (Syracuse and Abers, 2006). The older subducting slab (30–45) (Syracuse and Abers, 2006) in the central and southern regions is associated with a more shallow Wadati–Benioff zone and has down-dip compressive stress (Kubo and Fukuyama, 2003). Although some variability in slab geometry is present, the amplitude of average slab dip variations is less than 10° and trench geometry is approximately linear (Syracuse and Abers, 2006). Subduction geometry in the northern and central parts of the subduction system is approximately 2-D (Fig. 1b). Trench-perpendicular convergence velocity increases toward the south and varies from approximately 5 to 8 cm/yr (Syracuse and Abers, 2006). Radiometric dating and tectonic reconstructions suggest that subduction in the Ryukyu system initiated around 55 Ma (Faure et al., 1988; Karig, 1973; Jarrard, 1986).

3. Modeling approach

3.1. Thermomechanical and olivine fabric models

Recently, Long et al. (2007) presented a suite of 2-D viscous flow models for anisotropy development in the Ryukyu subduction zone and compared splitting predictions from these models to observations. In their approach, a region of B-type fabric was added to the model where the splitting data seem to

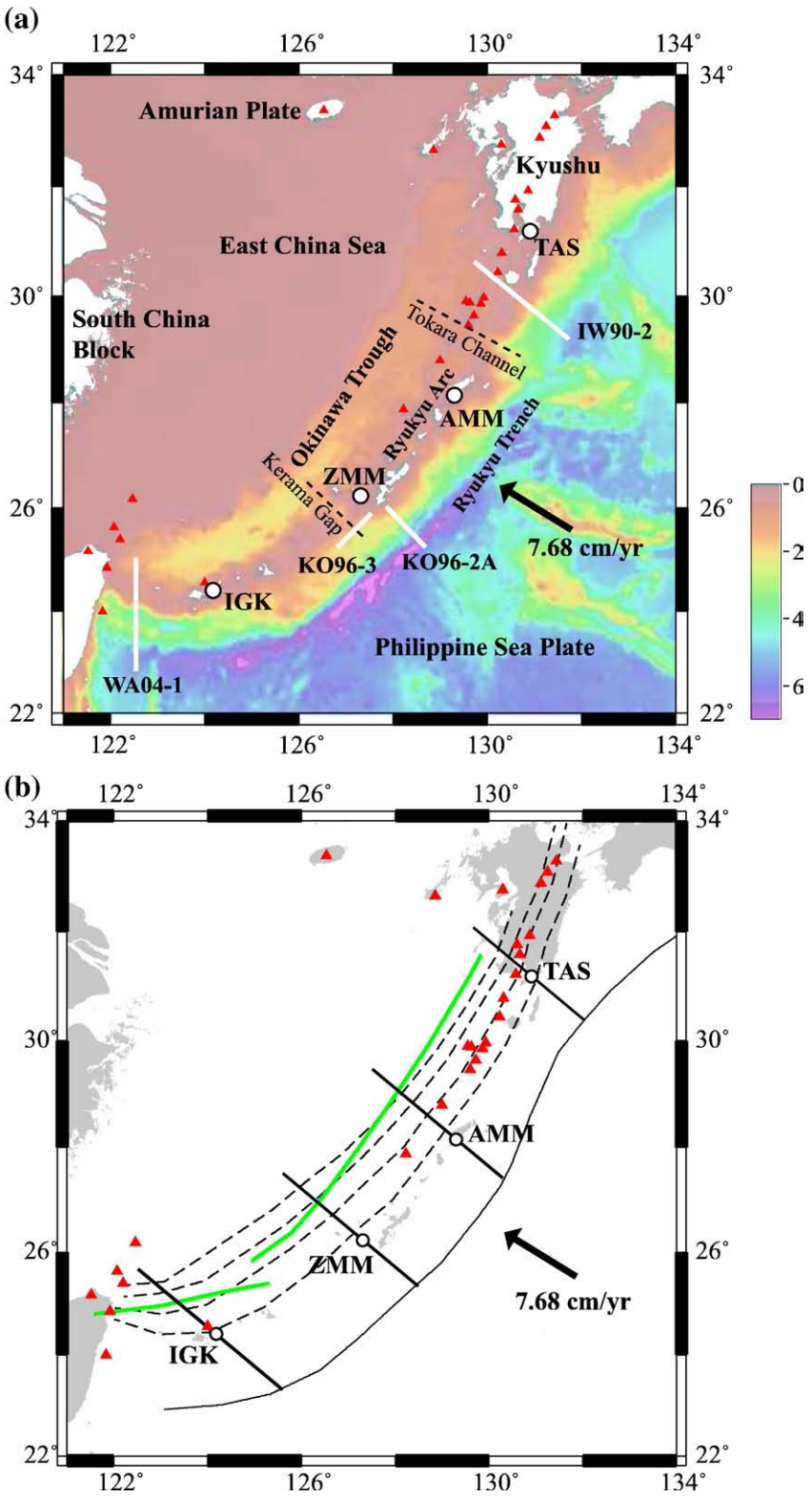

Fig. 1. Bathymetry (Smith and Sandwell, 1997), tectonic setting (a), and slab geometry (Syracuse and Abers, 2006) (b) of the Ryukyu subduction system. F-net stations considered in this study are denoted with white circles (a and b) (Long and van der Hilst, 2005, 2006). Quaternary volcanic centers are denoted with red triangles (a and b) (Siebert and Simkin, 2002). Black arrows denote relative plate motion between the Philippine Sea Plate and Amurian Plate from the plate model HS3-Nuvel1A (a and b) (Gripp and Gordon, 2002). Dashed lines represent left-lateral strike-slip faults (a). White lines show the location of refraction profiles that provide insights into the shallow structure of the fore-arc mantle (a): IW90-2 (Iwasaki et al., 1990), KO96-2A and KO96-3 (Kodaira et al., 1996), and WA04-1 (Wang et al., 2004). Slab contours (contour interval = 50 km) from (Syracuse and Abers, 2006) are denoted with black dashed lines (b). Thick black solid lines show the location of model profiles, whereas the thin line denotes the location of the trench (b). The axis of the Okinawa Trough is denoted by thick green lines (b).

require it. However, their models did not explicitly incorporate the physics of the olivine fabric transition. In this work, we take similar approach to (Long et al., 2007) but predict the location of the B-type transition with thermomechanical models that include partial coupling in the fore-arc mantle and experimentally-based rheological and fabric-transition parameters (Kneller et al., 2007). We also explore a more realistic range of slab geometries.

We implement the kinematic-dynamic steady-state approach described by (Kneller et al., 2007) (see Fig. 2a). The mantle wedge is treated as an infinite Prandtl number fluid with a wet composite olivine rheology. These models include viscous dissipation, depth-dependent shear heating along the upper 70 km of the slab-wedge interface, and parameterized partial coupling in the fore-arc mantle. Partial coupling is accomplished by reducing the magnitude of the velocity boundary condition along the slab-wedge interface in the fore-arc mantle and simulates the effects of weak materials (e.g. serpentinite) and/or brittle processes (e.g. aseismic creep). The magnitude of partial coupling is denoted by γ and is equal to the ratio of reduced velocity V_{red} over convergence velocity V_{slab} (Kneller et al., 2007). For all cases considered in this work model parameters include a convergence velocity V_{slab} equal to 8.42 cm/yr (Syracuse and Abers, 2006), an age of the incoming lithosphere equal to 43 Ma (Syracuse and Abers, 2006), and a shear heating gradient equal to 5 mW/m^2/km. The magnitude γ and depth D of partial coupling are variable. All other model parameters are identical to those used by (Kneller et al., 2007).

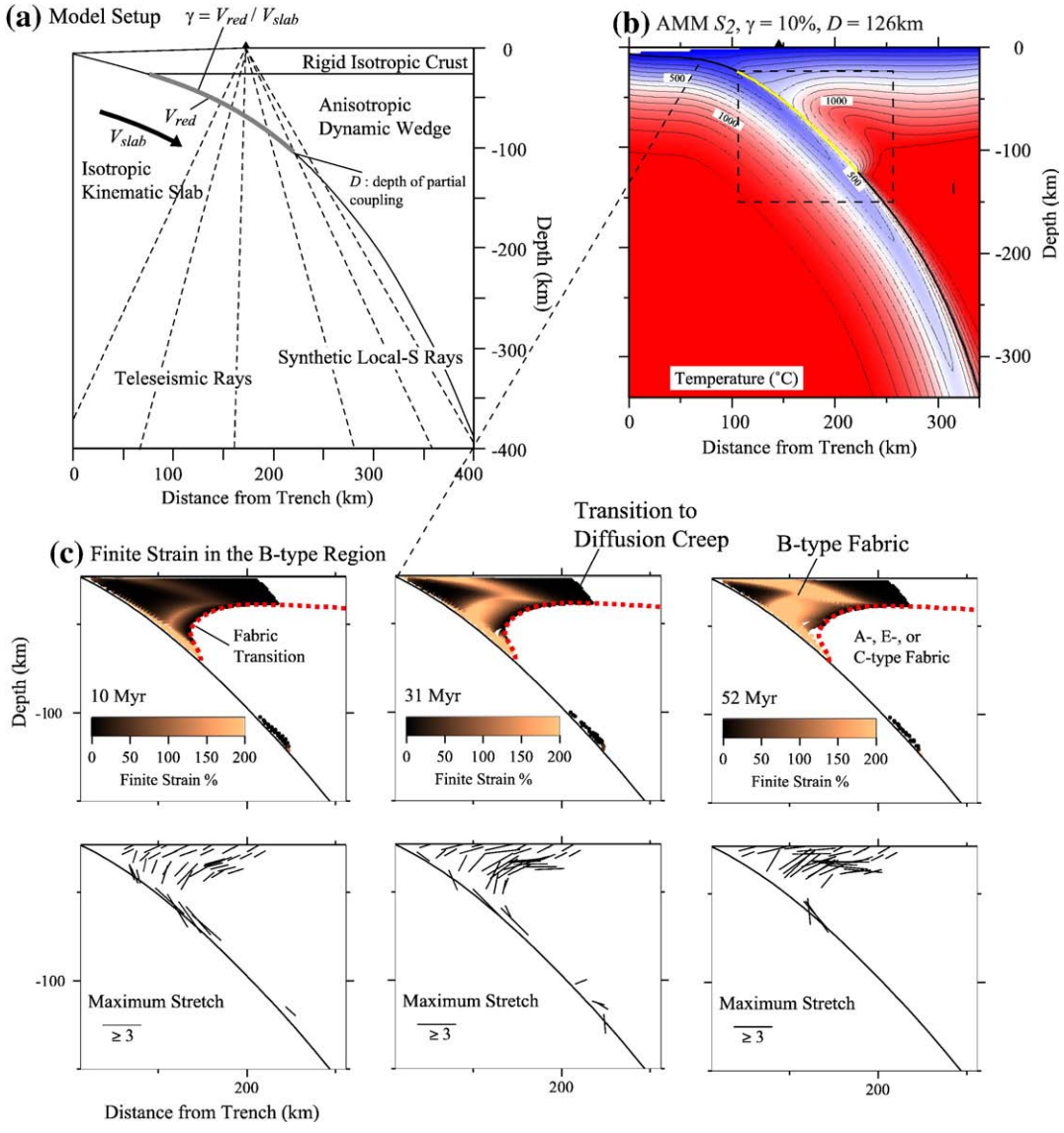

Fig. 2. Model setup, general ray geometry (a), and examples of output from high-resolution subduction zone models (b and c). The gray line in (a) denotes the partially coupled zone where the magnitude of the velocity boundary condition is reduced from V_{slab} to V_{red}. The magnitude of viscous coupling is defined by γ (see text). The contour interval used in (b) is 100 °C, and the dashed isotherm denotes the maximum *B*–*C* transition temperature (see text). The depth of the partially coupled zone is denoted by *D*. Steady-state thermal structure (b) and *B*-type fabric development (c) is shown for cross section AMM with slab model S_2, γ = 10%, and *D* = 126 km. The *B*-type fabric transition used for these cases is approximately 800 °C. Note that significant *B*-type fabric develops in the core of the fore-arc mantle by 20 to 30 Myr of deformation.

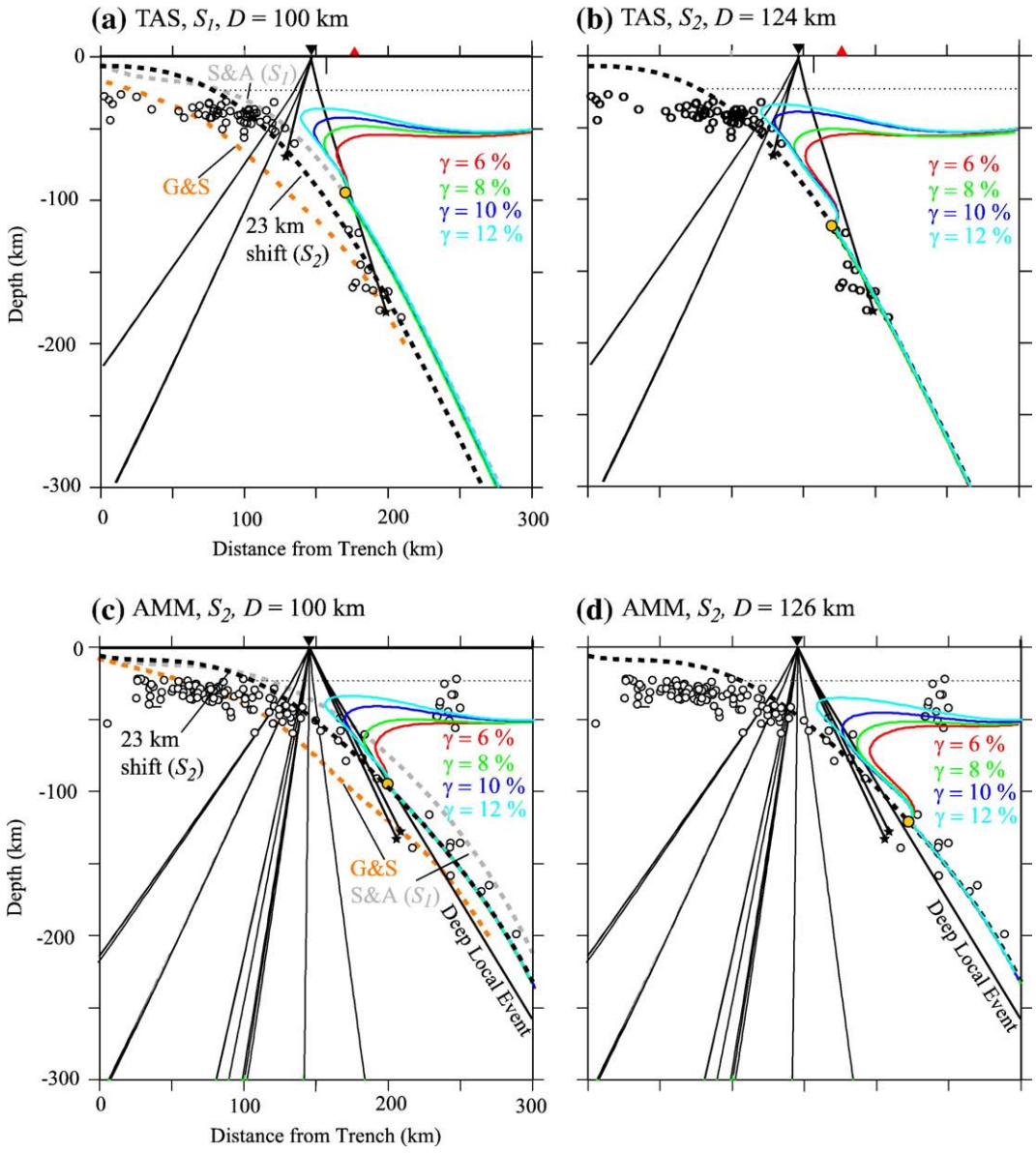

Fig. 3. Teleseismic and local-S ray geometry, slab models, and predicted *B*-type transition for cross sections TAS (a and b) and AMM (c and d). Colored lines in the mantle wedge show 900 ◦C isotherms (i.e. maximum *B*-type transition temperature) for a range of coupling parameters. F-net stations are denoted by black triangle. Red triangles denote nearby volcanic centers. Hypocenters of relocated earthquakes from the EHB catalog are denoted by open circles (Engdahl et al., 1998). Dashed lines correspond to various slab models considered in study: S_1 (S&A, light gray) is from (Syracuse and Abers, 2006), S_2 (black) is shifted 23 km relative to S_1, and S_3 (G&S, orange) is from (Gudmundsson and Sambridge, 1998). The depth of full coupling is denoted with an orange circle. Results are shown for a range of partial coupling magnitudes γ. For station TAS, results are shown for slab models S_1 and S_2 and decoupling depths that give rise to temperatures greater than 900 ◦C beneath the volcanic center. For cross section AMM, where no volcanic centers are located within a 75-100 km radius, results are shown for slab model S_2 and different decoupling depths.

The distribution of olivine fabric is determined using calculated temperature. Theoretical models, laboratory experiments, and natural observations show that the transition to B-type fabric will occur at temperatures ranging from 650–900 °C below a shear stress of 100 MPa (Katayama and Karato, 2006). We use a maximum B-type transition temperature of 900 °C. Below this temperature, B-type fabric is assumed to dominate and seismically fast directions align perpendicular to the flow direction. At higher temperatures low-stress fabrics are assumed to dominate, which have flow-parallel seismically fast directions (e.g. A-,C-, or E-type).

Spatially averaged finite strain calculations are used as a proxy for the magnitude and direction of olivine lattice preferred orientation. Finite strain axes are calculated in over 20,000 passive tracers using a 4th order Runge–Kutta scheme following the approach described (Kneller et al., 2007). Each 5 km increment is treated as a transversely isotropic (TI) medium (i.e. hexagonally symmetric) (Chevrot, 2000; Chevrot and van der Hilst, 2003; Browaeys and Chevrot, 2004). The hexagonally symmetric part of the elastic tensor for olivine aggregates accounts for approximately 90% of elastic properties (Browaeys and Chevrot, 2004). Material that crosses a fabric

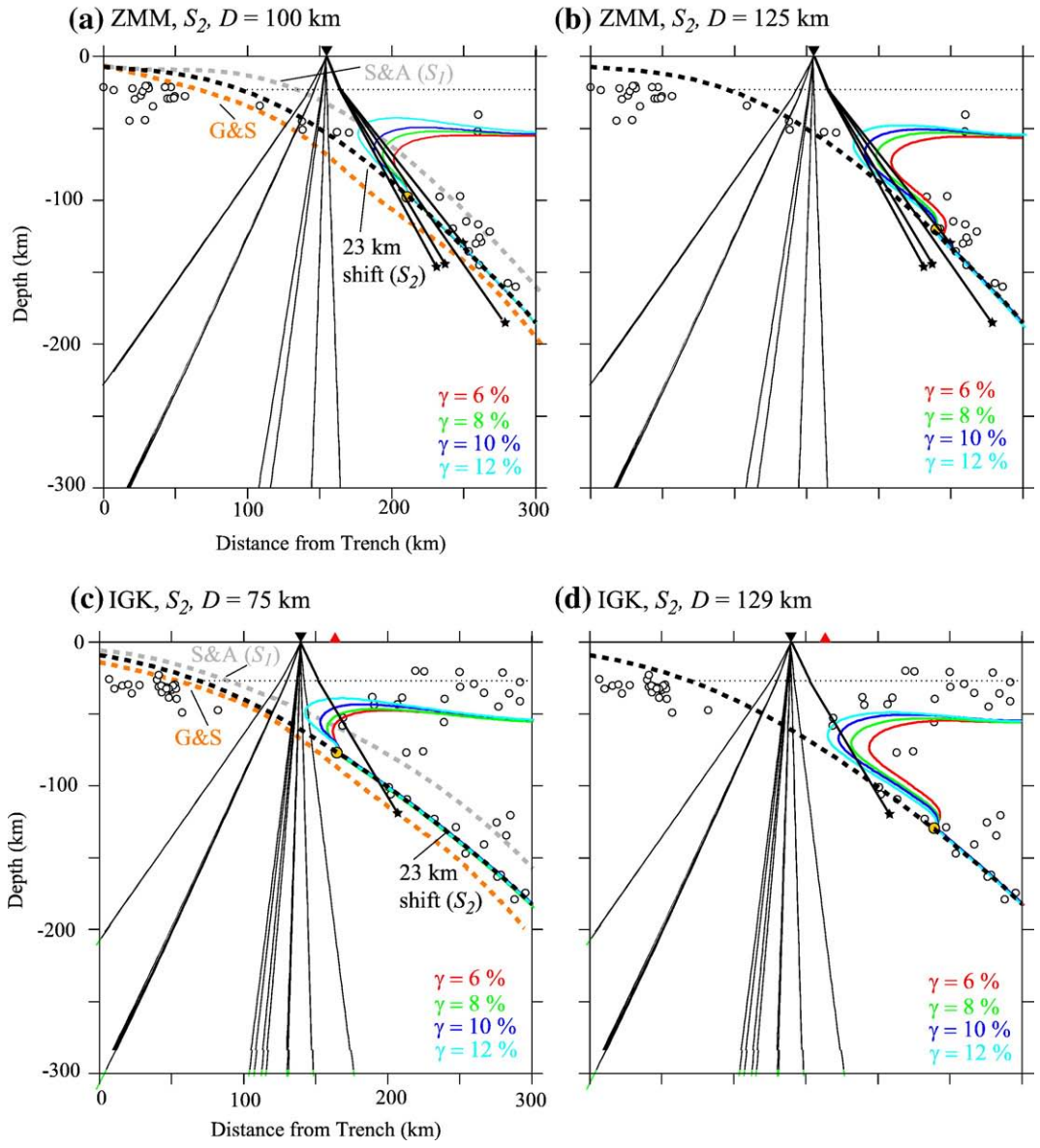

Fig. 4. Teleseismic and local-S ray geometry, slab models, and predicted B-type transition for cross sections ZMM (a and b) and IGK (c and d). Figure description is the same as in Fig. 3. For both ZMM and IGK, results are shown for slab model S_2 and different decoupling depths. The presence of a volcanic center behind station IGK suggests temperatures greater than 800◦ in the arc mantle. This requirement is met for decoupling depths less than 75 km and deep decoupling with γ greater than 12%. The distance between ZMM and the closest volcanic center is 200 km.

transition has finite strain set equal to zero. An example of thermal and strain calculations is shown in Fig. 2. For all cases considered in this study, finite strain calculations are shown after 52 Myr of deformation, a period of time that is less than the maximum estimated age of the Ryukyu arc (Jarrard, 1986).

With A- and E-type olivine fabrics (dry to moderate water content and low stress) the fast symmetry axis will align approximately perpendicular to the maximum stretch axes (Jung and Karato, 2001; Katayama et al., 2005; Jung et al., 2006; Katayama and Karato, 2006). At high water content and low-stress conditions slip occurs primarily on (100) and the fast symmetry axis will align approximately perpendicular to the shear plane giving rise to C-type fabric. All of these low-stress olivine fabrics (A-, C-, and E-type) produce seismically fast directions that align approximately parallel to maximum stretch axes when ray paths are steep and the flow geometry is dominated by horizontal shear (Jung and Karato, 2001; Jung et al., 2006), a situation that is consistent with the cases considered in this study. In regions dominated by stretching-parallel fabrics (A-, C- or E-type), we assume that the fast symmetry axis of the TI medium is parallel to the average dip of the maximum stretch axis. At low-temperature and wet conditions slip occurs primary on (010) and the fast symmetry axis of the TI medium aligns perpendicular to the shear direction in the shear plane (Jung and Karato, 2001; Katayama and Karato, 2006). In regions dominated by this B-type fabric, the symmetry

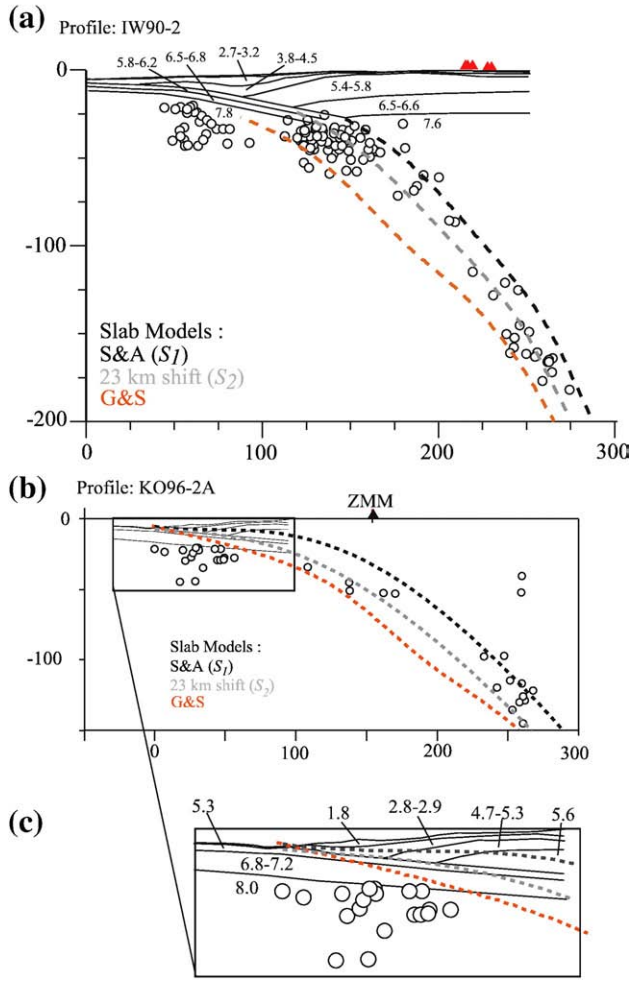

Fig. 5. Comparison between slab models and P-wave velocity (km/s) structure along profiles IW90-2 (a) and KO92-2A (b). Profiles are define in Fig. 1a. These refraction profiles provide important constraints on the shallow structure of the fore-arc mantle and suggest that the slab surface is located between slabs model S_1 and S_2 in the northern part of the arc and along cross section ZMM. The fore-arc slab surfaces of slab S_3 (G&S) are not consistent with refraction studies and overpredict the thickness of the anisotropic fore-arc mantle.

axis is set to be perpendicular to the maximum stretch axis but contained in the shear plane. Therefore, the fast axis is parallel to the strike of the trench, or out of the plane in Fig. 2c.

The maximum S-wave anisotropy for natural olivine aggregates ranges from 5 to 15% with an average of around 6.5% (Ismaïl and Mainprice, 1998). We explore this range of observed elastic properties by formulating TI media with 9, 11.6, and 14.4% anisotropy. Elastic stiffness tensors for the TI media are defined using a Voigt average of two components (Mainprice, 1990): (1) the hexagonally symmetric part of the elastic tensor of a single crystal of olivine and (2) the elastic tensor of an isotropic reference mantle. The relative amounts of these components are allowed to vary, which leads to media with variable anisotropy strengths. The isotropic reference mantle is composed of a weighted average of the isotropic parts of the elastic tensors of enstatite and olivine for a mixture of 30% enstatite and 70% olivine (Browaeys and Chevrot, 2004).

We compared the finite-strain based fabric model used in this work to a more complex model of LPO development (Kneller, 2007), D-Rex, which includes dislocation glide, dynamic recrystallization, grain boundary sliding, and variable olivine and enstatite volume fraction (Lassak et al., 2006; Kaminski et al., 2004). With D-Rex, LPO development is a function of the velocity field, critically resolved shear stresses for specific slip systems, and three free fabric development parameters. These free parameters control dynamic recrystallization and diffusive deformation processes that limit fabric strength: λ^* (nucleation parameter), M^* (grain boundary mobility), and χ (threshold volume for the activation of grain-boundary sliding) (Lassak et al., 2006; Kaminski et al., 2004). Both the finite-strain approach and D-Rex show a similar distribution and relative magnitude of olivine fabric. The maximum S-wave anisotropy produced in the B-type region by the D-Rex model with 90% olivine volume fraction and experimentally constrained parameters ($\lambda^*=0.2$; $M^*=200$; $\chi=6$) is 10–11%.

3.2. Slab geometry

We construct four cross sections that intersect F-net stations where observations suggest relatively simple anisotropy (AMM, IGK, TAS, and ZMM; see Fig. 2b). Refraction studies from the northern and central Ryukyu arc show that crustal thickness in the arc-fore-arc region is around 23 to 25 km (Iwasaki et al., 1990; Kodaira et al., 1996). Refraction studies from the southern edge of the subduction system show a slightly thicker crustal thickness (25–30 km) (Wang et al., 2004). We use a uniform crustal thickness of 23 km for models constructed along profiles in the northern and central Ryukyu arc (TAS, AMM, ZMM) (Fig. 1). A uniform crustal thickness of 27 km is used along profile IGK, which is located in the southern part of the arc.

We consider several models of slab surfaces based on intermediate depth seismicity: (1) S_1, slab surfaces from (Syracuse and Abers, 2006), which are consistently located at the upper surface of the Wadati–Benioff zone, (2) S_2 slab surfaces that are shifted 23 km deeper at intermediate depth relative to (Syracuse and Abers, 2006), and (3) S_3, slab surfaces from the RUM model (Gudmundsson and Sambridge, 1998), which tend to be located at the base of the Wadati–Benioff zone. The 23 km shift with respect to S_1 is the approximate thickness of the Wadati–Benioff zone in the Ryukyu arc and is a measure of the maximum uncertainty in the depth of the slab surface (Syracuse and Abers, 2006). The subduction zone geometries considered in this study are shown in Figs. 3 and 4.

Refraction studies of deep fore-arc structure provide important constraints on slab geometry above 100 km depth (Iwasaki et al., 1990; Kodaira et al., 1996; Wang et al., 2004). A convergence-parallel seismic refraction profile is available in the northern part of the Ryukyu fore-arc arc, 500 km south of station TAS (Iwasaki et al., 1990) (Figs. 1 and 5). This study suggests that the slab surface from (Gudmundsson and Sambridge, 1998) (S_3) is least accurate in the fore-arc region. In the central part of the arc a convergence-parallel refraction profile (Kodaira et al., 1996) is juxtaposed to the model cross section ZMM (Figs. 1 and 5). This profile and an additional

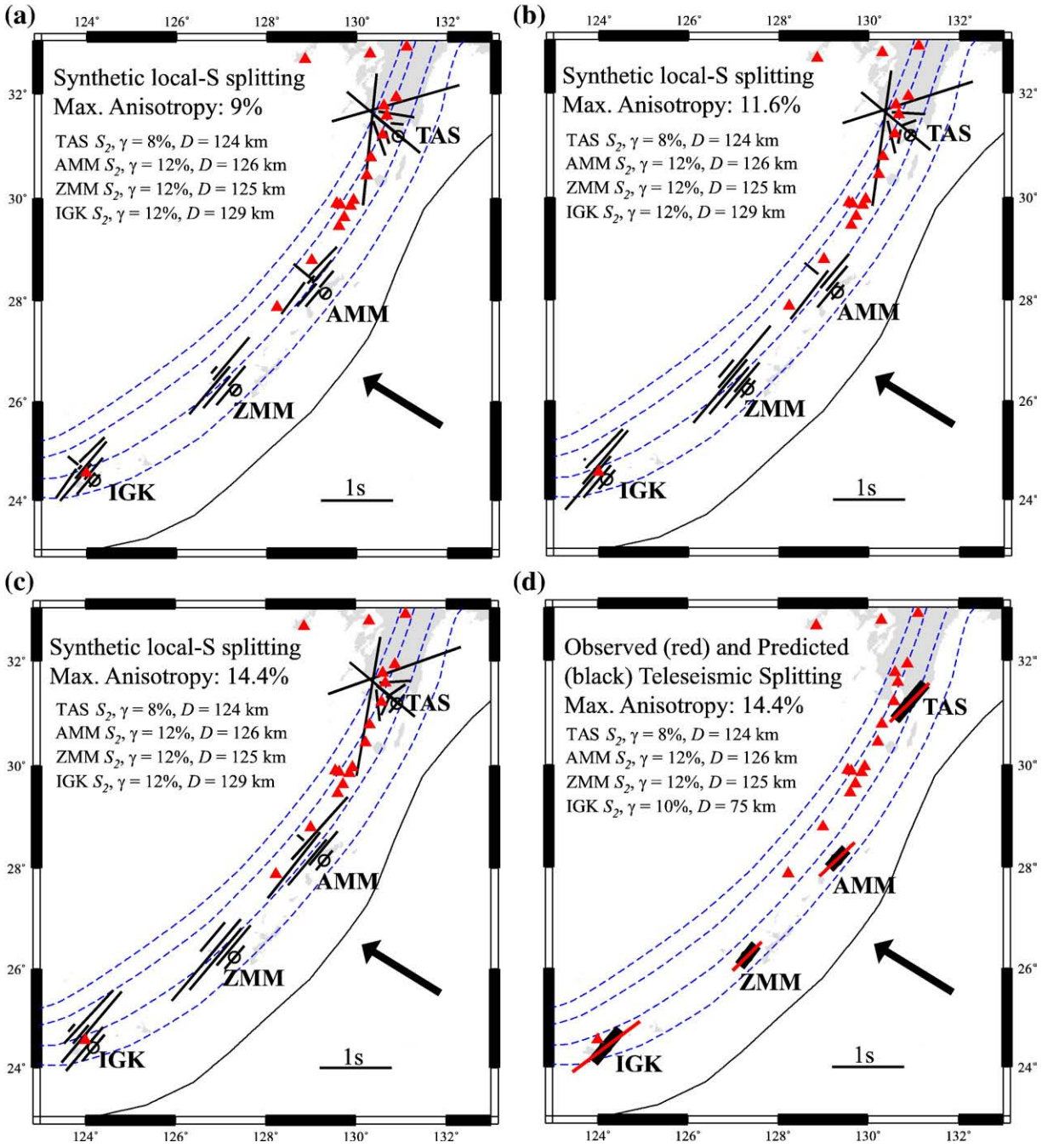

Fig. 6. Calculated local-S (a–c) and teleseismic (d) shear wave splitting for subduction zone models that give rise to the closest match with observations. Black lines denote calculated fast vibration directions and magnitudes. Local-S predic- tions are shown for a range of maximum S-wave anisotropy in the B-type region (5.6% anisotropy in A-type region). Local-S splitting calculations for each station are performed for a range of backazimuths and incidence angles. Observed teleseismic splitting (thin red lines) are compared to results from models with maximum S-wave anisotropy approximately equal to the maximum for natural olivine aggregates (14.4%) (thick black lines) (d).

convergence-perpendicular profile (Kodaira et al., 1996) (Fig. 1) also suggest that the slab surfaces from (Gudmundsson and Sambridge, 1998) are too deep in the fore-arc region.

3.3. Predicted splitting calculations

We predict splitting based on the calculated distribution of finite strain in the wedge with the following procedure. We trace rays through the model domain using a straight-ray approximation in 5 km depth increments. Rays are traced in three dimensions but we use the one-dimensional velocity model iasp91 (Kennett and Engdahl, 1991) as a background and isotropic velocities vary only with depth. For each 5-km depth increment in the mantle wedge, we calculate quasi-S velocities and fast/slow polarizations. The down-going slab and over-riding plates are isotropic. We use approximate expressions for

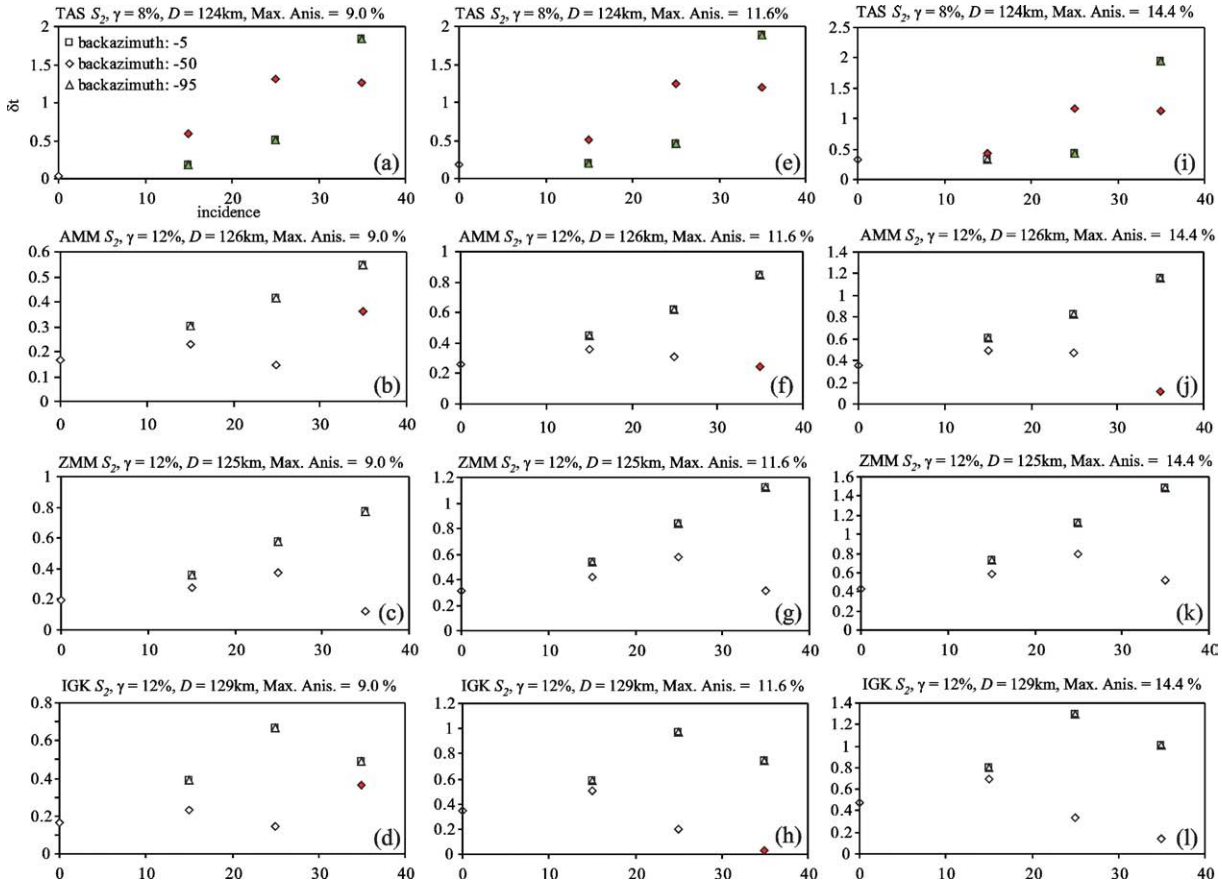

Fig. 7. Local-S splitting parameters as a function of backazimuth and incidence angle for cases shown in Fig. 5. Delay time is denotes by δt. Open symbols denote trench-parallel fast directions, whereas green and red symbols denote oblique and trench-perpendicular fast directions respectively.

V_{qS_1} and V_{qS_2}, and δt for an arbitrarily oriented transversely isotropic medium and an arbitrarily oriented ray path as described by (Chevrot and van der Hilst, 2003) and (Long et al., 2007). Splitting intensity is calculated for each depth increment using the relationship

$$s_i = \delta t \sin(2(\theta - \phi)) \quad (1)$$

where s_i is the splitting intensity for a single layer, δt is the delay time, φ is the fast polarization direction, and θ is the incoming polarization angle (Chevrot, 2000). Splitting intensity at the surface is then obtained by summing incremental contributions.

We predict splitting intensities for two sets of rays. For teleseismic splitting, we use ray geometries that correspond to actual source–receiver pairs in data set of (Long and van der Hilst, 2005). In order to capture the range of splitting that might be observed for local slab earthquakes, however, we create synthetic local ray paths that sample the deep fore-arc mantle over a range of backazimuths and incoming polarization angles. Our methodology for predicting splitting intensities is limited to low frequencies, and the low-frequency dataset of (Long and van der Hilst, 2006) is limited to a fairly small number of observations at the stations considered in this study. For this reason, we prefer to predict local splitting for generic local ray paths with a range of backazimuths and incidence angles. This provides good sampling of the entire wedge, and also is representative of the types of local-S rays in the splitting dataset. These generic predictions can then be compared to the local splitting observed by (Long and van der Hilst, 2006). A sketch of typical ray paths used in the modeling approach is shown in Fig. 2a.

Average splitting parameters for teleseismic arrivals are calculated from the phase delay (fast direction) and amplitude (delay time) of the best sin(2θ) fit to the predicted splitting intensity versus incoming polarization angle (Chevrot, 2000). The incoming polarization angles for the teleseismic rays were measured from seismograms (Long and van der Hilst, 2005).

Fig. 8. A comparison between observed and predicted splitting intensity as a function of incoming polarization angle for teleseismic phases. Cases are shown from models that give rise to the best match with observations at each station. For station TAS results are shown for slab models S_1 and S_2, whereas with other stations results are shown only for slab model S_2. Open circles and 2-σ error bars denote observations from (Long and van der Hilst, 2005). Thick dashed curves are best sin(2θ) fits to observed splitting intensity. Colored lines are sin(2θ) fits to calculated splitting intensity for variable maximum S-wave anisotropy. Thin dashed lines in (d) show results from the antigorite serpentinite model (see text).

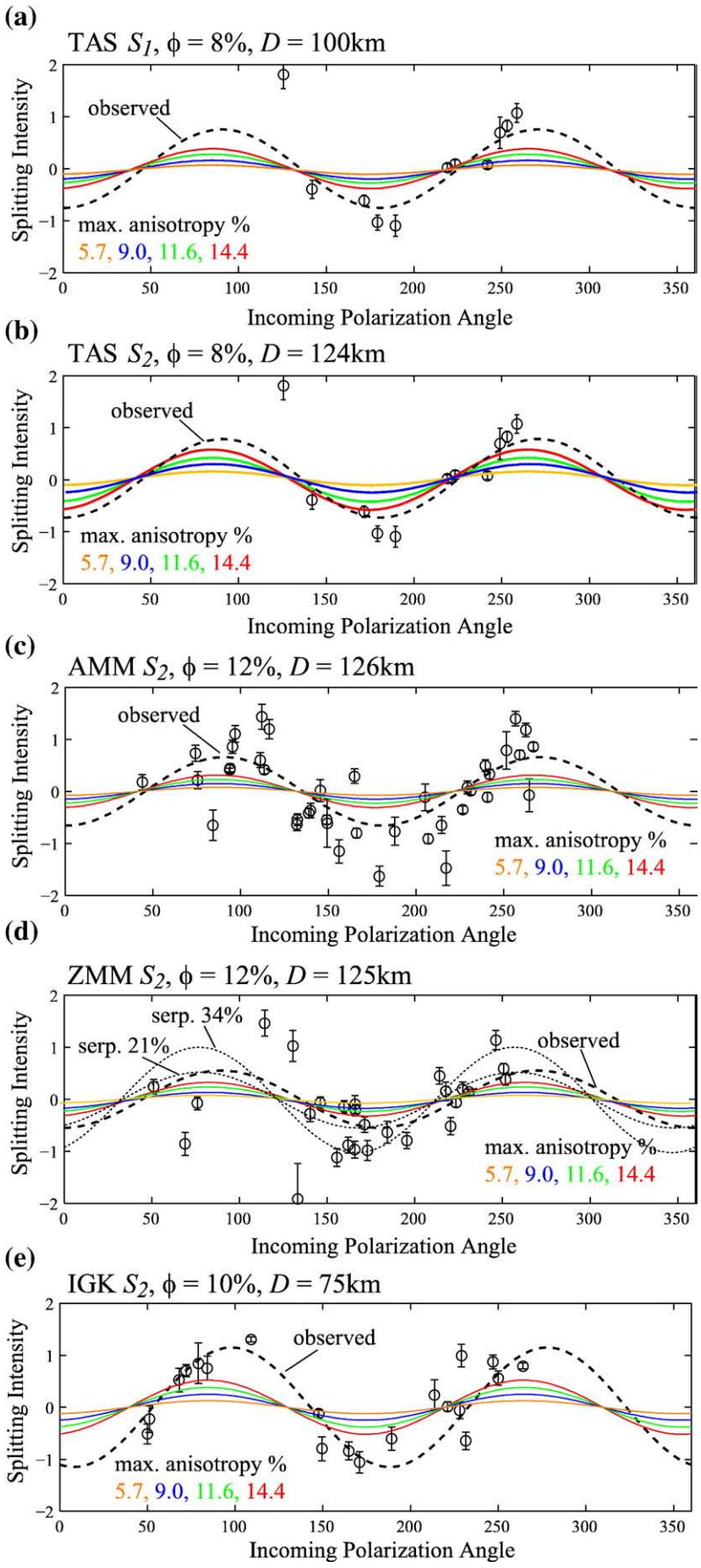
(a)
TAS S_1, ϕ = 8%, D = 100km
observed
max. anisotropy %
5.7, 9.0, 11.6, 14.4
Splitting Intensity
Incoming Polarization Angle
(b)
TAS S_2, ϕ = 8%, D = 124km
observed
max. anisotropy %
5.7, 9.0, 11.6, 14.4
Splitting Intensity
Incoming Polarization Angle
(c)
AMM S_2, ϕ = 12%, D = 126km
observed
max. anisotropy %
5.7, 9.0, 11.6, 14.4
Splitting Intensity
Incoming Polarization Angle
(d)
ZMM S_2, ϕ = 12%, D = 125km
serp. 34%
serp. 21%
observed
max. anisotropy %
5.7, 9.0, 11.6, 14.4
Splitting Intensity
Incoming Polarization Angle
(e)
IGK S_2, ϕ = 10%, D = 75km
observed
max. anisotropy %
5.7, 9.0, 11.6, 14.4
Splitting Intensity
Incoming Polarization Angle

For the synthetic local-S rays we use a similar approach. However, the initial polarization direction for our synthetic local ray paths is arbitrary; in practice, the initial polarization will depend on the focal mechanism of the earthquake. Therefore, we calculate splitting intensity over a range of all possible incoming polarization angles and we predict average splitting parameters from this range.

4. Results

4.1. The B-type transition and ray geometry

The depth and magnitude of partial coupling are the most important parameters for the distribution of B-type fabric conditions (Kneller et al., 2007). As the magnitude of coupling increases, the B-type transition moves closer to the trench (Figs. 3 and 4). Both teleseismic and local-S rays travel exclusively through the B-type region for slab model S_2 and coupling magnitudes that ranges from 6 to 12%. The sampling of B-type conditions by local-S rays shows a greater sensitivity to the magnitude of partial coupling and slab geometry for all cases considered in this study.

The path length of both teleseismic and local rays through the fore-arc mantle is largest at station TAS where slab dip is relatively steep at shallow depth (Fig. 3a). In the central and southern parts of the arc at stations AMM, ZMM, and IGK slab dip decreases at shallow depth and the fore-arc mantle is relatively thin (Figs. 3 and 4). Slab model S_1 for AMM and ZMM is associated with a fore-arc mantle that is too thin to produce the observed delay times. If model S_1 accurately reflects slab geometry, the source of anisotropy may be distributed through the upper part of the subducting slab, a thin fore-arc mantle, and overriding crust (Figs. 3 and 4). Although this scenario is possible, the $\sin(2\theta)$ relationship between splitting intensity and incoming polarization angle suggests a source that resembles a simple single anisotropic layer. Slab model S_2 provides a reasonable match with shallow seismic structure and intermediate depth seismicity and is associated with a thicker fore-arc mantle (Figs. 3 and 4).

The presence of volcanic centers behind stations TAS and IGK requires temperatures exceeding 800–900 °C (Grove et al., 2006) in the wet arc mantle. Figs. 3a, b, 4c, and d show coupling parameters that give rise to temperatures greater than 800–900 °C beneath volcanic centers and a large B-type region through which rays almost exclusively travel.

4.2. Observed and predicted splitting

We predict local-S splitting parameters with synthetic rays that have a range of backazimuths (−5 to −95°) and mantle incidence angles (0 to 35°) (Fig. 2a) and sample the deep fore-arc mantle (Figs. 3 and 4). Models of shear wave splitting in the rapidly flowing hot arc and back-arc mantle show that a maximum S-wave anisotropy of 5–6% provides a close match with observations (Fischer et al., 2000; Lassak et al., 2006). The large delay times associated with local-S phases suggest the presence of a larger magnitude of anisotropy in the cold corner of the Ryukyu wedge (>9%). Since rock fabric strength and maximum S-wave anisotropy in the mantle wedge are unknown, we explore a range of values that are consistent with naturally deformed olivine aggregates.

Figs. 6 and 7 show predicted local-S splitting for models with coupling parameters and slab geometry that provide the best match with observations. Results are shown for maximum S-wave anisotropy in the B-type region equal to 9%, 11.6%, and 14.4%. Anisotropy in the A-type region is set equal to 5.6%. At stations AMM, ZMM, and IGK the predicted direction of local splitting is consistently trench parallel with trench-perpendicular splitting occurring only for incidence angles greater than 35°. The magnitude of splitting is dependent on incidence angle and backazimuth with larger trench-parallel delay times associated with larger incidence angles and backazimuths approximately parallel and perpendicular to the trench (Fig. 7). Maximum predicted local-S delay times of 0.8 s to 1.5 s are obtained for maximum anisotropy equal to 9% and 14.4%, respectively.

High- and low-frequency local-S observations at the stations considered in this study show a mixture of trench-parallel and oblique fast directions and delay times that range from 0.35 to 1.65 s (Long and van der Hilst, 2006). Low-frequency observations are associated with primarily trench-parallel fast directions and have larger delay times relative to high-frequency events. Of the 34 non-null local-S events reported by (Long and van der Hilst, 2006), only two trench-perpendicular fast directions were observed. The predicted pattern of local-S splitting is very similar to observed patterns. Predicted local-S fast directions consist of mixture of primarily trench-parallel orientations and secondary trench-perpendicular and oblique orientations (Figs. 6 and 7). Furthermore, predicted local-S delay times range from 0.2 to 2 s depending on maximum anisotropy, backazimuth, and incidence angle (Fig. 7).

The predicted splitting intensity for teleseismic phases shows a similar pattern to the observations (Fig. 8). Predicted fast directions are within 5–15° of observed values. In the northern region of the arc, where the fore-arc mantle reaches maximum thickness, the predicted teleseismic delay time is within 40 to 80% of the observed values for maximum anisotropies ranging from 9 to 14.4% and slab model S_2 (Figs. 8 and 9). In the central and southern parts of the arc, the fore-arc mantle is thin and B-type fabric accounts for 20 to 50% the observed splitting magnitude for maximum anisotropy ranging from 9 to 14.4% (Figs. 8 and 9 b). The closest match between observed teleseismic splitting and the predictions from the B-type model is obtained with a maximum anisotropy equal to 14.4% in the B-type region (Fig. 6d). Slab model S_3 gives rise to the thickest region of B-type fabric and matches the trench-parallel teleseismic delay times almost perfectly. However, we consider this model to be less accurate than S_1 and S_2 based on shallow seismic structure and intermediate depth seismicity (e.g. Fig. 5).

5. Crustal anisotropy, fore-arc serpentinization, and teleseismic splitting

Measurements of crustal anisotropy are not available for Ryukyu. However, studies from the Japan and Cascadia

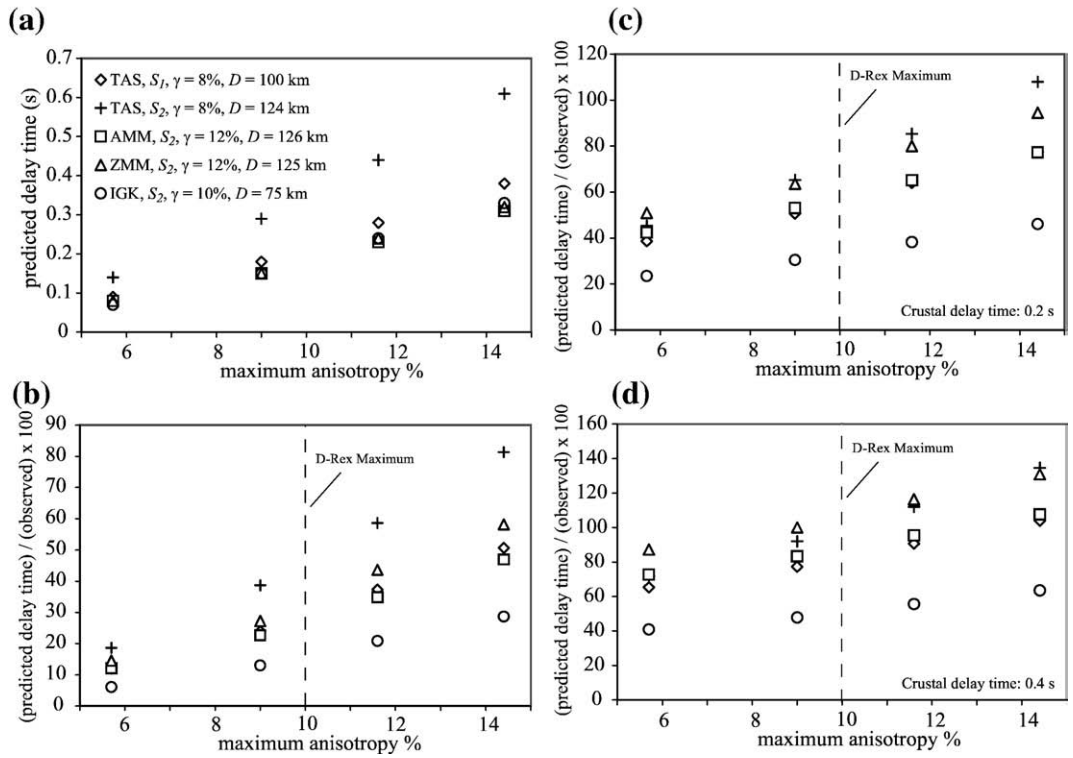

Fig. 9. A comparison between observed and predicted teleseismic splitting param-eters. Plots include predicted delay time (a), predicted delay time normalized to observed delay time (b), predictions from (b) but with the addition of 0.2 s of crustal delay time (c), and predictions from (b) but with the addition of 0.4 s of crustal delay time (d). The dashed lines denote the approximate maximum S-wave anisotropy for an olivine aggregate with 90% olivine in the fore-arc mantle according to calculations from self-consistent models of LPO development (see text).

subduction systems suggest that crustal anisotropy in the Ryukyu arc will be less than 0.2–0.4 s (Currie et al., 2001; Kaneshima, 1990). Possible causes of crustal anisotropy include LPO of crustal minerals and shape preferred orientation from cracks in the crust that align perpendicular to the compression direction (Currie et al., 2001; Hiramatsu and Ando, 1996). We explore the effects of crustal anisotropy by adding the maximum trench-parallel delay times observed in the crust of the Cascadia fore arc (Currie et al., 2001) to the teleseismic predictions. Approximately 60–100% of the observed trench-parallel delay time is explained by a model with B-type fabric (7–11% max. anisotropy) and a crust with 0.4 s of trench-parallel delay time at stations TAS, AMM, and ZMM (Fig. 9d). However, a model with maximum observed anisotropy and maximum observed trench-parallel crustal anisotropy can only account for 60% of the observed trench-parallel delay time at station IGK (Fig. 9d).

The teleseismic phases considered in this study sample the coldest region of the fore-arc mantle where thermal calculations suggests that antigorite serpentinite may play an important role in controlling fabric development and seismic anisotropy (Ulmer and Trommsdorff, 1995; Bromiley and Pawley, 2003; Komabayashi et al., 2005; Kneller et al., 2007) (Fig. 10a and b). Laboratory experiments show that foliated antigorite serpentinite is associated with maximum S-wave anisotropy as large as 38% and a slow hexagonal symmetry axis that aligns perpendicular to the foliation plane (Kern, 1993; Kern et al., 1997) (Fig. 10a).

If the foliation of antigorite serpentinite is near vertical, the cold tip of the fore-arc mantle will be an anisotropic medium with a horizontal and trench-perpendicular slow symmetry axis. This may give rise to the large magnitude trench-parallel splitting with a $\sin(2\theta)$ relationship between splitting intensity and incoming polarization angle of teleseismic phases (Fig. 10b). Finite strain calculations from models with a range of rheological parameters show near vertical finite strain axes in the core of the fore-arc mantle, which is consistent with near vertical foliation (Fig. 10b).

Unfortunately, modeling serpentinite deformation and associated seismic anisotropy is difficult due limited experimental constraints for the ductile rheology and elastic properties of serpentine. We therefore performed a simple calculation to estimate the splitting due to a serpentinized wedge at station ZMM. We constructed an elastic tensor with the same symmetry as the muscovite elastic tensor and maximum S-wave anisotropies of 21%, 27%, and 35%. Assuming that the anisotropic geometry is uniform and the slow symmetry axis is perpendicular to the trench, we predicted 0.6–1 s of trench-parallel teleseismic splitting (Fig. 8d). This matches or exceeds the observed delay times for this station and suggests that serpentinite may play a role in controlling anisotropy in the cold tip of the fore-arc mantle.

6. Discussion and conclusions

The B-type fabric model provides a reasonable reproduction of both the magnitude and trench-parallel pattern of shear wave splitting associated with local-S phases (Fig. 6). These phases

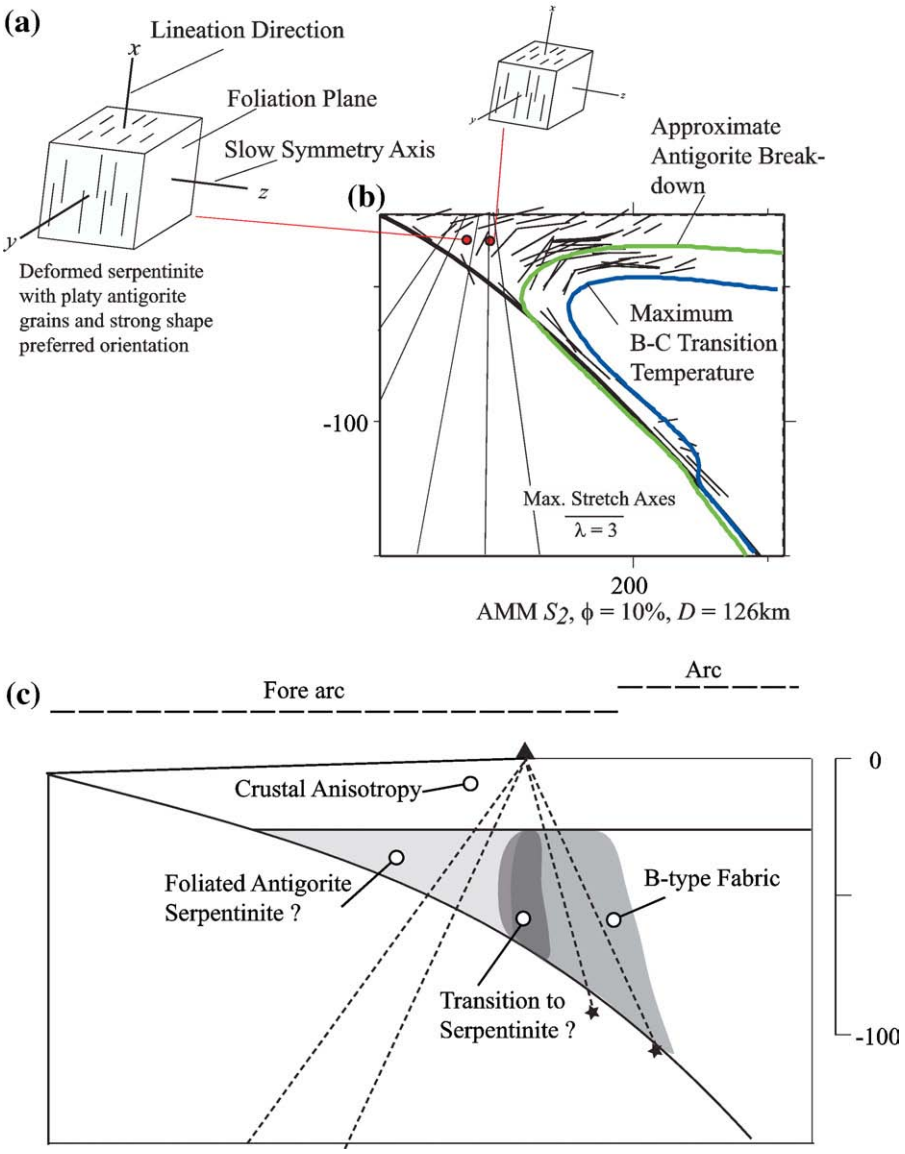

Fig. 10. Preliminary antigorite serpentinite model for large magnitude trench-parallel teleseismic splitting (a and b) and main conclusions from this work (c). Laboratory observations suggest that foliated antigorite serpentinite will be associated with a slow symmetry axis perpendicular to the foliation plane (Kern, 1993; Kern et al., 1997) (a). Hypothetical blocks of foliated serpentinite with orientations based on finite strain calculations are shown in (a) and (b). Calculated antigorite stability (≈700 °C, green line), B-type transition (blue line), and maximum stretch axes are shown in (b). Teleseismic phases sample the cold corner of the fore-arc mantle where thermal condition are suitable for antigorite stability and maximum stretch axis in the core of the fore-arc are approximately vertical (b). This may give rise to trench-parallel fast directions and large magnitude simple anisotropy (b). B-type fabric reproduces splitting for deep local phases (c). However, other mechanism are mostly responsible for large magnitude trench-parallel splitting associated with teleseismic phases that sample the cold tip of the fore-arc mantle (c).

sample the deep fore-arc mantle of the Ryukyu subduction system where geodynamic models predict extensive B-type fabric development. The models presented in this work also show that maximum S-wave anisotropy in the B-type region must be greater than 9% to reproduce the magnitude of local splitting. This value is larger than the average maximum S-wave anisotropy for natural olivine aggregates but exists well within the range of observed values (5–15%) (Ismaïl and Mainprice, 1998) and is consistent with models of LPO development in peridotite (Kaminski et al., 2004).

In order for the B-type model to provide a close match with observations, maximum anisotropy in the B-type region must be larger than anisotropy in the A-type region. Maximum anisotropy is unknown and depends on olivine volume fraction, grain boundary mobility, and physicochemical conditions (Jung et al., 2006; Kaminski et al., 2004). These factors may spatially vary within the wedge giving rise to variable maximum anisotropy. Fabric development within the B-type region occurs over much longer time scales relative to the warmer regions of the mantle wedge. This may give rise to a stronger fabric and larger intrinsic anisotropy in the B-type region.

The B-type fabric model with maximum S-wave anisotropy close to the maximum observed value for olivine aggregates accounts for less than 50% of the observed teleseismic trench-

parallel delay time for most slab geometries considered in this study (Fig. 9b). The discrepancy between observed and predicted teleseismic delay time may be explained by crustal anisotropy or the presence of foliated antigorite serpentinite in the tip of the fore-arc mantle. We also cannot rule out a contribution from the slab, although we consider it less likely. Any contribution to the splitting signal from slab anisotropy would have to have a fast direction parallel to anisotropy in the mantle wedge, since the simple teleseismic splitting patterns observed for Ryukyu (Long and van der Hilst, 2005) are inconsistent with two anisotropic layers with significantly different fast directions. Fossil spreading directions for the Philippine Plate suggest that anisotropy in the slab is more likely to have a fast direction oblique to the trench (Sdrolias et al., 2004) but the spreading history is complex and the resulting anisotropy is not straightforward. These splitting observations cannot rule out a contribution from the slab of up to 0.4 s.

Variations in slab geometry may produce a component of trench-parallel flow and stretching (Kneller and van Keken, 2008, in revision). However, we assume that in Ryukyu mantle wedge the impact of variable geometry is small since along-strike slab dip variations do not exceed 10°, average slab dip is greater than 45°, and the trench is approximately linear in the northern and central regions. 3-D flow associated with small-scale convection (Honda and Saito, 2003) is also considered unlikely since most ray paths are confined to the cold corner where high viscosity inhibits free convection (Honda and Saito, 2003). Slab rollback (Buttles and Olson, 1998; Kincaid and Griffiths, 2003), oblique subduction, and trench-parallel motion of the overriding plate (Hall et al., 2000) may produce a component of trench-parallel flow throughout the arc, back-arc, and fore-arc mantle. These mechanisms are also considered to be unlikely causes of trench-parallel splitting in Ryukyu since slab rollback velocity is low (<1 cm/yr) (Heuret and Lallemand, 2005), the curvature in the trench is small, convergence is orthogonal, and faults with strike-slip motion are oriented perpendicular to the trench.

The preferred alignment of melt-filled cracks, pockets, or networks may produce flow-normal fast seismic anisotropy (Hiramatsu and Ando, 1996; Kendall et al., 2005). The presence of partial melt may also cause the seismically fast axes of olivine grains to preferentially align perpendicular to flow (Holtzman et al., 2003). These melt-related mechanisms may play an important role in localized hot regions of the mantle. Although we cannot rule out a contribution from melt for deeper local phases, this mechanism is considered unlikely due to the absence of volcanism throughout large regions of the central and southern parts of the Ryukyu subduction system.

The calculations presented in this work show that the B-type fabric model explains the magnitude and trench-parallel orientation associated with local-S phases that travel through the deep fore-arc mantle of the Ryukyu subduction system (Fig. 10c). B-type fabric alone cannot explain the large magnitude trench-parallel shear wave splitting in the cold tip of the fore-arc mantle. Alternative explanations involve an anisotropic continental crust or the presence of a highly anisotropic material such as foliated antigorite serpentinite.

Acknowledgments

We thank Geoff Abers and Ellen Syracuse for providing cross sections of seismicity and slab surfaces from the Ryukyu subduction system. We also thank Shun-ichiro Karato, Ikuo Katayama, and Philip Skemer for helpful discussions on olivine fabric transitions. We acknowledge the Japanese National Research Institute for Earth Science and Disaster Prevention as the source for the data used in this study. Finally, we thank the two anonymous reviewers for constructive reviews. This research was supported by the National Science Foundation.

References

Anderson, M.L., Zandt, G., Triep, E., Fouch, M., Beck, S., 2004. Anisotropy and mantle flow in the Chile-Argentina subduction zone from shear wave split-ting analysis, Geophys. Res. Lett. 31. doi:10.1029/2004GL020906.

Bromiley, G., Pawley, A., 2003. The stability of antigorite in the systems MgO–SiO_2–H_2O (MSH) and MgO–Al_2O_3–SiO_2–H_2O (MASH): the effects of Al^{3+} substitution on high-pressure stability. Am. Mineral. 88, 99–1082.

Browaeys, J.T., Chevrot, S., 2004. Decomposition of the elastic tensor and geo-physical applications. Geophys. J. Int. 159, 667–678.

Buttles, J., Olson, P., 1998. A laboratory model of subduction zone anisotropy. Earth Planet. Sci. Lett. 164, 245–262.

Chevrot, S., 2000. Multichannel analysis of shear wave splitting. J. Geophys. Res. 105, 21579–21590.

Chevrot, S., van der Hilst, R.D., 2003. On the effects of a dipping axis of symmetry on shear wave splitting measurements in a transversely isotropic medium. Geophys. J. Int. 152, 497–505.

Currie, C.A., Cassidy, J.F., Hyndman, R.D., 2001. A regional study of shear wave splitting above the Cascadia subduction zone: margin-parallel crustal stress. Geophys. Res. Lett. 28, 659–662.

Engdahl, E.R., van der Hilst, R., Buland, R., 1998. Global teleseismic earth-quake relocation with improved travel times and procedures for depth determination. Bull. Seismol. Soc.Am. 88, 722–743.

Faure, M., Monie, P., Fabbri, O., 1988. Microtectonics and ^{39}Ar–^{40}Ar dating of high pressure metamorphic rocks of the south Ryukyu Arc and their bearings on the pre-Eocene geodynamic evolution of Eastern Asia. Tectonophysics 156, 133–143.

Fischer, K.M., Parmentier, E.M., Stine, A.R., Wolf, E., 2000. Modeling anisotropy and plate-driven flow in the Tonga subduction zone back arc. J. Geophys. Res. 105, 181–191.

Fournier, M., Fabbri, O., 2001. Regional seismicity and on-land deformation in the Ryukyu arc: implication for kinematics of opening of the Okinawa Trough. J. Geophys. Res. 106, 13751–13768.

Frese, K., Trommsdorff, V., Kunze, K., 2003. Olivine [100] normal to foliation: lattice preferred orientation in prograde garnet peridotite formed at high H_2O activity, Cima di Gagnone (Central Alps). Contrib. Mineral. Petrol. 145, 75–86.

Gripp, A., Gordon, R., 2002. Young tracks of hot spots and current plate velocities. Geophys. J. Int. 150, 321–361.

Grove, T.L., Chatterjee, N., Parman, S.W., Médard, E., 2006. The influence of H_2O on mantle wedge melting. Earth Planet Sci. Lett. 249, 74–89.

Gudmundsson, O., Sambridge, M., 1998. A regionalized upper mantle (RUM) seismic model. J. Geophys. Res. 103, 7121–7136.

Hall, C.E., Fischer, K.M., Parmentier, E.M., Blackman, D.K., 2000. The influence of plate motions on three-dimensional back arc mantle flow and shear wave splitting. J. Geophys. Res. 105, 28009–28033.

Heuret, A., Lallemand, S., 2005. Plate motions, slab dynamics and back-arc deformation. J. Geophys. Res. 149, 31–51.

Hiramatsu, Y., Ando, M., 1996. Seismic anisotropy near source region in subduction zones around Japan. Phys. Earth Planet. Inter. 95, 237–250.

Hiramatsu, Y., Ando, M., Tsukuda, T., Ooida, T., 1998. Three-dimensional image of the anisotropic bodies beneath central Honshu, Japan. Geophys. J. Int. 135, 801–816.

Holtzman, B.K., Kohlstedt, D.L., Zimmerman, M.E., Heidelback, F., Hiraga, T., Hustoft, J., 2003. Melt segregation and strain partitioning: implications for seismic anisotropy and mantle flow. Science 301, 1227–1230.

Honda, S., Saito, M., 2003. Small-scale convection under the back-arc occurring in the low viscosity wedge. Earth Planet. Sci. Lett. 216, 703–715.

Ismaïl, B.W., Mainprice, D., 1998. An olivine fabric database: an overview of upper mantle fabrics and seismic anisotropy. Tectonophysics 196, 145–157.

Iwasaki, T., Hirata, N., Kanazawa, T., Melles, J., Suyehiro, K., Urabe, T., Moller, M.J., Shimamura, L.H., 1990. Crustal and upper mantle structure in the Ryukyu Island Arc deduced from deep seismic sounding. Geophys. J. Int. 102, 631–651.

Jarrard, R.D., 1986. Relations among subduction parameters. Rev. Geophys. 24, 217–284.

Jung, H., Karato, S., 2001. Water-induced fabric transition in olivine. Science 293, 1460–1463.

Jung, H., Katayama, I., Jiang, Z., Hiraga, T., Karato, S., 2006. Effect of water and stress on the lattice-preferred orientation of olivine. Tectonophysics 421, 1–22.

Kamata, H., Kodama, K., 1999. Volcanic history and tectonics of the Southwest Japan Arc. Island Arc 8, 393–403.

Kaminski, E., Ribe, N.M., Browaeys, J.T., 2004. D-Rex, a program for calculation of seismic anisotropy due to crystal lattice preferred orientation in the convective upper mantle. Geophys. J. Int. 158, 744–752.

Kaneshima, S., 1990. Origin of crustal anisotropy; shear wave splitting studies in Japan. J. Gephys. Res. 95, 11121–11133.

Karig, D.E., 1973. Plate convergence between the Philippines and Ryukyu islands. Mar. Geol. 14, 153–168.

Katayama, I., Karato, S., 2006. Effect of temperature on the B- to C-type olivine fabric transition and implication for flow pattern in subduction zones. Phys. Earth Planet. Inter. 157, 33–45.

Katayama, I., Karato, S., Brandon, M., 2005. Evidence of high water content in the deep upper mantle inferred from deformation microstructures. Geology 33, 613–616.

Kendall, J.M., Stuart, G., Ebinger, C., Bastow, I., K., D., 2005. Magma-assisted rifting in Ethiopia. Nature 433, 146–148.

Kennett, B., Engdahl, E., 1991. Traveltimes for global earthquake location and phase identification. Geophys. J. Int. 105, 429–465.

Kern, H., 1993. P- and S-wave anisotropy and shear-wave splitting at pressure and temperature in possible mantle rocks and their relation to the rock fabric. Phys. Earth Planet. Inter. 78, 245–256.

Kern, H., Liu, B., Popp, T., 1997. Relationship between anisotropy of P and S wave velocities and anisotropy of attenuation in serpentinite and amphibolite. J. Geophys. Res. 102, 3051–3065.

Kincaid, C., Griffiths, R., 2003. Laboratory models of the thermal evolution of the mantle during rollback subduction. Nature 425, 58–62.

Kneller, E., Geodynamic Insights into Patterns of Shear Wave Anisotropy in Subduction Zones, 2007, PhD Dissertation, University of Michigan.

Kneller, E.A., van Keken, P.E., 2008. The effect of three-dimensional slab geometry on deformation in the mantle wedge: implications for shear wave anisotropy, Geochem. Geophys. Geosyst. 9, Q01003, doi:10.1029/2007GC001677.

Kneller, E., van Keken, P., in revision. Trench-parallel flow and seismic anisotropy in the Mariana and Andean subduction systems, Nature.

Kneller, E., van Keken, P., Katayama, I., Karato, S., 2007. Stress, strain, and B-type olivine fabric in the fore-arc mantle: sensitivity tests using high-resolution steady-state subduction zone models. J. Geophys. Res. 112. doi:10.1029/2006JB004544.

Kneller, E.A., van Keken, P.E., Karato, S., Park, J., 2005. B-type olivine fabric in the mantle wedge: insights from high-resolution non-Newtonian subduction zone models. Earth Planet. Sci. Lett. 237, 781–797.

Kodaira, S., Iwasaki, T., Urabe, T., Kanazawa, T., Egloff, F., Makris, J., Shimamura, H., 1996. Crustal structure across the middle Ryukyu trench obtained from ocean bottom seismographic data. Tectonophysics 263, 39–60.

Komabayashi, T., Hirose, K., Funakoshi, K., Takafuji, N., 2005. Stability of phase A in antigorite (serpentine) composition determined by in situ X-ray pressure observations. Phys. Earth Planet. Inter. 151, 276–289.

Kubo, A., Fukuyama, E., 2003. Stress field along the Ryukyu Arc and the Okinawa trough inferred from moment tensors of shallow earthquakes. Earth Planet. Sci. Lett. 210, 305–316.

Lassak, T.M., Fouch, M.J., Hall, C.E., Kaminski, E., 2006. Seismic characterization of mantle flow in subduction systems: can we resolve a hydrated mantle wedge? Earth Planet. Sci. Lett. 243, 632–649.

Long, M., van der Hilst, R., 2006. Shear wave splitting from local events beneath the Ryukyu arc: trench-parallel anisotropy in the mantle wedge. Phys. Earth Planet. Inter. 155, 300–312.

Long, M., van der Hilst, R., 2005. Upper mantle anisotropy beneath Japan from shear wave splitting. Phys. Earth Planet. Inter. 151, 1346–1358.

Long, M., Hager, B., de Hoop, M., van der Hilst, R., 2007. Two-dimensional modelling of subduction zone anisotropy with application to southwestern Japan. Geophys. J. Int. 170, 839–856.

Mainprice, D., 1990. A Fortran program to calculate seismic anisotropy from the lattice preferred orientation of minerals. Comput. Geosci. 16, 385–393.

McKenzie, D., 1979. Finite deformation during fluid flow. Geophys. J. R. Astron. Soc. 58, 689–715.

Mizukami, T., Wallis, S.R., Yamamoto, J., 2004. Natural examples of olivine lattice preferred orientation patterns with a flow-normal *a*-axis maximum. Nature 427, 432–436.

Nakajima, J., Hasegawa, A., 2004. Shear-wave polarization anisotropy and subduction-induced flow in the mantle wedge of northeastern Japan. Earth Planet. Sci. Lett. 225, 365–377.

Nakajima, J., Shimizu, J., Hori, S., Hasegawa, A., 2006. Shear-wave split-ting beneath the southwestern Kurile arc and northeastern Japan arc: A new insight into mantle return flow. Geophys. Res. Lett. 33. doi:10.1029/2003JB002718.

Nakamura, M., 2004. Crustal deformation in the central and southern Ryukyu Arc estimated from GPS data. Earth Planet. Sci. Lett. 217, 389–398.

Nishimura, S., Hashimoto, M., Andob, M., 2004. A rigid block rotation model for the GPS derived velocity field along the Ryukyu arc. Phys. Earth Planet. Inter. 142, 185–203.

Sdrolias, M., Roest, W.R., Muller, R.D., 2004. An expression of Philippine Sea plate rotation: the Parece Vela and Shikoku Basins. Tectonophysics 394, 69–86.

Shinjo, R., 1999. Geochemistry of high Mg andesites and the tectonic evolution of the Okinawa Trough-Ryukyu arc system. Chem. Geol. 157, 69–88.

Shinjo, R., Woodhead, J., Hergt, J., 2000. Geochemical variation within the northern Ryukyu Arc: magma source compositions and geodynamic implications. Contrib. Mineral. Petrol. 140, 263–282.

Siebert, L., Simkin, T., 2002. Volcanoes of the world: An illustrated catalog of holocene volcanoes and their eruptions Global Volcanism Program Digital Inf. Ser., GVP-3, Smithsonian Institution., Washington, D. C. (Available at http://www.volcano.si.edu/world/).

Skemer, P., Katayama, I., Karato, S., 2006. Deformation fabrics of the Cima di Gagnone Peridotite Massif, Central Alpes, Swizerland: evidence of deformation under water-rich conditions at low temperatures. Contrib. Mineral. Petrol. 152, 43–51.

Smith, G.P., Wiens, D.A., Fischer, K.M., Dorman, L.M., Webb, S.C., Hildebrand, J.A., 2001. A complex pattern of mantle flow in the Lau Back arc. Science 292, 713–716.

Smith, W., Sandwell, D., 1997. Global seafloor topography from satellite altimetry and ship depth sounding. Science 277, 1957–1962.

Syracuse, E.M., Abers, G.A., 2006. Global compilation of variations in slab depth beneath arc volcanoes and implications. Geochem. Geophys. Geosystem 7. doi:10.1029/2005GC001045.

Taira, A., 2001. Tectonic evolution of the Japanese island arc system. Annu. Rev. Earth Planet. Sci. 29, 109–134.

Ujiie, K., 2002. Evolution and kinematics of an ancient decollement zone, melange in the Shimanto accretionary complex of Okinawa Island. Ryukyu Arc, J. Struc. Geol. 24, 937–952.

Ulmer, P., Trommsdorff, V., 1995. Serpentine stability to mantle depth and subduction-related magmatism. Science 268, 858–861.

Wang, T.K., Lin, C., Liu, S., Wang, C., 2004. Crustal structure of the southern-most Ryukyu subduction zone: OBS, MCS and gravity modeling. Geophys. J. Int. 157, 147–163.

Yang, X., Fischer, K.M., Abers, G., 1995. Seismic anisotropy beneath the Shuma-gin Islands segment of the Aleutian-Alaska subduction zone. J. Geophys. Res. 100, 18165–18177.